Elastoinertial chains in a two-dimensional turbulent flow

Rahul Singh,[1,*] Mohit Gupta,[1,2,†] Jason R. Picardo,[3,‡] Dario Vincenzi,[4,§] and Samriddhi Sankar Ray[1,‖]
[1]*International Centre for Theoretical Sciences, Tata Institute of Fundamental Research, Bangalore 560089, India*
[2]*School of Physics and Astronomy, University of Minnesota, Minneapolis, Minnesota 55455, USA*
[3]*Department of Chemical Engineering, Indian Institute of Technology Bombay, Mumbai 400076, India*
[4]*Université Côte d'Azur, CNRS, LJAD, Nice 06100, France*

(Received 26 August 2019; accepted 28 February 2020; published 18 May 2020)

The interplay of inertia and elasticity is shown to have a significant impact on the transport of filamentary objects, modeled by bead-spring chains, in a two-dimensional turbulent flow. We show how elastic interactions among inertial beads result in a nontrivial sampling of the flow, ranging from entrapment within vortices to preferential sampling of straining regions. This behavior is quantified as a function of inertia and elasticity and is shown to be very different from free, noninteracting heavy particles, as well as inertialess chains [Picardo *et al.*, Phys. Rev. Lett. **121**, 244501 (2018)]. In addition, by considering two limiting cases, of a heavy-headed and a uniformly inertial chain, we illustrate the critical role played by the mass distribution of such extended objects in their turbulent transport.

DOI: 10.1103/PhysRevE.101.053105

I. INTRODUCTION

The study of the dynamics of a long filamentary object in a turbulent flow is fairly recent. In particular, studies on the deformation [1–4] and buckling [5] of fibers, as well as on their usefulness as a probe for the statistical properties of a turbulent flow [6,7], have led to the development of new ideas in the area of turbulent transport which go beyond the spherical point-particle approximation.

The dynamics of such filamentary objects becomes particularly intriguing when their length extends beyond the dissipation scale of the turbulent flow; the mean flow velocity sampled by the object is then dependent on its instantaneous shape, and this couples translation to flow-induced deformation. (The situation is considerably simpler for a subdissipation scale object, as its center of mass behaves like a tracer, independently of its internal dynamics.) Recently, the work of Picardo *et al.* [8], which studied long elastic chains consisting of inertialess tracers linked by springs, revealed a new mechanism by which such objects preferentially sample the flow: unlike a collection of noninteracting tracers, which distribute homogeneously, these chains selectively occupy the vortical regions of a two-dimensional turbulent flow, with a nontrivial dependence on the elasticity (quantified by the Weissenberg number Wi) and typical interbead separations in the chain.

This behavior of elastic chains is in contrast to the well-known preferential sampling of straining regions exhibited by noninteracting, heavy particles (whose inertia is measured through the Stokes number St). More popularly known as "preferential concentration," this phenomenon has been the subject of extensive research in the last decade [9–16], motivated by its relevance to a diverse range of physical processes, from transport in particle-laden sprays [17] to collision-driven growth of droplets in warm clouds [18,19].

It is critical to appreciate that the mechanisms of preferential sampling by the elastic inertia-less chains and the noninteracting, inertial particles are fundamentally different. In the former, it is the elasticity of the links which allows such chains to extend, coil up, and be trapped in vortices, whereas for the latter the dissipative dynamics and centrifugal expulsion from vortices lead to particles concentrating in straining regions. This contrast naturally leads us to investigate the dynamics of a heavy elastic chain, which serves as a model for an extensible filamentary object that possesses both inertia and elasticity, as is the case in most physical situations. In addition, by varying the masses of the particles that compose a chain, we can study the effect of an inhomogeneous mass distribution along the chain itself.

Therefore, such a chain provides a simple way to account for the simultaneous effects of inertia, elasticity, and fluid drag in models of filamentary objects, such as algae in marine environments [20], biofilaments (actin and microtubules, for instance) [21], and swimming microorganisms [22–24]. Of course, such applications would require the consideration of additional effects, such as an active swimming velocity and interchain interactions. Nevertheless, the basic ideas elucidated below, in particular the competing effects of inertia and elasticity on preferential sampling, should remain relevant and help pave the way for future studies.

II. MODEL

Towards this end, we consider an *elastoinertial chain*, i.e., a sequence of heavy spherical particles—henceforth called beads—which are connected to their nearest neighbors through elastic (phantom) links [see Fig. 1(a)] with an

*rahul.singh@icts.res.in
†mohit.gupta9607@gmail.com
‡jrpicardo@che.iitb.ac.in
§dario.vincenzi@unice.fr
‖samriddhisankarray@gmail.com

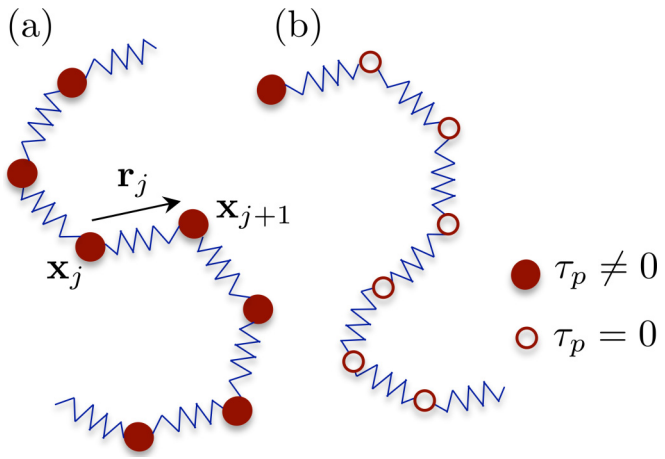

FIG. 1. A schematic of (a) a uniformly inertial and (b) a heavy-headed chain illustrating the notation used in the text.

associated timescale τ_E. The N_b beads that compose the chain have positions $\mathbf{x}_j$, $1 \leqslant j \leqslant N_b$, and each bead is characterized by the inertial relaxation time τ_p (defined precisely later) with which its velocity would relax to that of the fluid in the absence of elastic interactions with the neighboring beads. By incorporating the drag stemming from the advecting fluid velocity field $\mathbf{u}$ and the elastic forces on each bead, we obtain the equations of motion for the interbead separation vectors $\mathbf{r}_j = \mathbf{x}_{j+1} - \mathbf{x}_j$ with $1 \leqslant j \leqslant N_b - 1$ [see Fig. 1(a)]:

$$\tau_p \ddot{\mathbf{r}}_j = [\mathbf{u}(\mathbf{x}_{j+1}, t) - \mathbf{u}(\mathbf{x}_j, t) - \dot{\mathbf{r}}_j] - \frac{1}{4\tau_E}(2f_j\mathbf{r}_j - f_{j-1}\mathbf{r}_{j-1} - f_{j+1}\mathbf{r}_{j+1}) + \sqrt{\frac{r_0^2}{2\tau_E}}[\boldsymbol{\xi}_{j+1}(t) - \boldsymbol{\xi}_j(t)]. \quad (1)$$

Here the "link velocity" is denoted as $\dot{\mathbf{r}}_j = \dot{\mathbf{x}}_{j+1} - \dot{\mathbf{x}}_j$ and the "link acceleration" as $\ddot{\mathbf{r}}_j$. We use the FENE (finitely extensible nonlinear elastic) interaction $f_j = (1 - |\mathbf{r}_j^2|/r_m^2)^{-1}$, where r_m is the maximum interbead length, commonly used in polymer physics [25]. We also consider independent white noises $\boldsymbol{\xi}_j(t)$ acting on each bead, in order to set the equilibrium link-length, proportional to r_0, thereby preventing the chain from collapsing to a point object. Alternatively, this could be achieved without including fluctuations, by incorporating r_0 directly into the elastic forces, i.e., by replacing $-f_j\mathbf{r}_j$ with $-f_j\mathbf{r}_j(1 - r_0/|\mathbf{r}_j|)$ in Eq. (1). We have checked that the two formulations lead to similar sampling behaviors. The equation of motion for the center of mass $\mathbf{x}_c$ is given by

$$\tau_p \ddot{\mathbf{x}}_c = \left[\frac{1}{N_b}\sum_{j=1}^{N_b}\mathbf{u}(\mathbf{x}_j, t) - \dot{\mathbf{x}}_c\right] + \frac{1}{N_b}\sqrt{\frac{r_0^2}{2\tau_E}}\sum_{j=1}^{N_b}\boldsymbol{\xi}_j(t). \quad (2)$$

While in Eq. (1) the noise term is needed to set a nonzero equilibrium size, it has a negligible effect on the trajectory of the center of mass and produces only a small correction to its turbulent eddy diffusivity.

In Eqs. (1) and (2), we have taken τ_p, τ_E, and r_0 to be identical for all beads and links. Thus we obtain a uniformly inertial chain, which will be the main focus of our study. However, to explore the role of the mass distribution of the chain, we also consider a second case, in which all the inertia is concentrated in a single heavy end bead ($j = 1$), with the remainder of the chain composed of $N_b - 1$ inertia-less beads, as illustrated in Fig. 1(b). Such a "heavy-headed chain" pits the inertia of the head bead against the elasticity of its tail and serves as an ideal candidate to illustrate the effects of these competing forces. The equations of motion for the interbead links of such a heavy-headed chain are a specific instance of Eqs. (1) and (2) and are given by

$$\dot{\mathbf{r}}_j = \mathbf{u}(\mathbf{x}_{j+1}, t) - \mathbf{u}(\mathbf{x}_j, t) - \frac{1}{4\tau_E}(2f_j\mathbf{r}_j - f_{j-1}\mathbf{r}_{j-1} - f_{j+1}\mathbf{r}_{j+1}) + \sqrt{\frac{r_0^2}{2\tau_E}}[\boldsymbol{\xi}_{j+1}(t) - \boldsymbol{\xi}_j(t)], \quad \forall j \neq 1 \quad (3)$$

and for $j = 1$:

$$\dot{\mathbf{r}}_1 = \mathbf{u}(\mathbf{x}_2, t) + \frac{1}{4\tau_E}(f_2\mathbf{r}_2 - f_1\mathbf{r}_1) + \sqrt{\frac{r_0^2}{2\tau_E}}\boldsymbol{\xi}_2(t) - \dot{\mathbf{x}}_1. \quad (4)$$

The center of mass, which coincides with the head bead, obeys

$$\tau_p \ddot{\mathbf{x}}_1 = [\mathbf{u}(\mathbf{x}_1, t) - \dot{\mathbf{x}}_1] + \frac{1}{4\tau_E}f_1\mathbf{r}_1 + \sqrt{\frac{r_0^2}{2\tau_E}}\boldsymbol{\xi}_1(t). \quad (5)$$

Equations (1) to (5) complete the description of the dynamics of our two types of elastoinertial chains. This, of course, is a *minimal* description because, in order to keep the model as simple as possible, we have neglected certain effects that are not essential to our study. Hydrodynamic and excluded-volume interactions between the segments of a chain, although present in a real filament, are not expected to modify the dynamics qualitatively. As was shown in Ref. [8] for an inertial-less chain and as will be further demonstrated below for elastoinertial chains, preferential sampling in two-dimensional turbulence results from a dramatic difference in the configuration of the chain in straining and vortical regions (for instance, inertia-less chains are highly stretched in the former and coiled up in the latter [8]). This essential qualitative behavior would be affected only marginally by the aforementioned interactions. Collisions and hydrodynamic interactions between different chains as well as the back reaction of the chain dynamics on the flow would be relevant to the study of a suspension of chains, but less so to the present study, in which we focus on how a single chain samples a turbulent flow. Finally, our elastic links do not offer any resistance to bending, which ought to be important in any realistic modeling of an elastic filament [26]. The reason for disregarding it here is that, for an extended object advected by a turbulent flow, little is known even about just the interplay between its elasticity and inertia. Thus, the goal of our study is to understand this issue by considering a minimal model of an elastic filament that allows us to isolate the competing roles of inertia and elasticity. Refinements of the model, aimed at a more realistic description of an elastic filament, will naturally

have to consider its bending stiffness as an additional feature of the dynamics.

We immerse the elastoinertial chain in a two-dimensional, homogeneous, isotropic turbulent velocity field $\mathbf{u}$, which is obtained through direct numerical simulations (DNSs) of the incompressible ($\boldsymbol{\nabla}\cdot\mathbf{u}=0$) Navier-Stokes equation:

$$\partial_t\mathbf{u}+(\mathbf{u}\cdot\boldsymbol{\nabla})\mathbf{u}=-\boldsymbol{\nabla}p+\nu\nabla^2\mathbf{u}+\mathbf{f}-\mu\mathbf{u}. \tag{6}$$

Two-dimensional flows are particularly useful for investigating the competing effects of elasticity and inertia because of long-lived, coherent vortical structures, as we shall see later. We use a standard pseudospectral method to solve Eq. (6) on a 2π square periodic domain with $N^2=1024^2$ collocation points. We drive the flow to a turbulent, statistically steady state with an external forcing $\mathbf{f}=-F_0\sin(k_f x)\mathbf{e_y}$, where F_0 is the forcing amplitude and k_f sets the energy injection and typical vortex scale $l_f=2\pi k_f^{-1}$. The energy at large scales (due to an inverse cascade) is damped out by using an Ekmann term [27,28] with the coefficient of friction $\mu=10^{-2}$. The flow is characterized by the large eddy-turnover timescale $\tau_f=l_f/\sqrt{2E}$ and the short timescale $\tau_\eta=1/\sqrt{2\langle\omega^2\rangle}$ associated with enstrophy dissipation, where E is the mean kinetic energy of the flow and $\langle\omega^2\rangle$ is the mean enstrophy (averaged spatially over the domain and temporally over the statistically steady state). We set the coefficient of kinematic viscosity $\nu=1\times10^{-6}$, $k_f=5$, and $F_0=0.2$, giving $\tau_f=1.45$ and $\tau_\eta=0.35$.

As mentioned earlier, we study the dynamics of a single chain and its preferential sampling of the flow. However, we evolve 5×10^4 chains simultaneously with the purpose of illustrating preferential sampling visually as well as achieving high accuracy in the statistics of chain deformation and translation. The dynamics of the chains is determined by Eqs. (1) and (2) or (3) to (5). These are numerically integrated by a second-order Runge-Kutta scheme. Each chain consists of $N_b=10$ beads and has a maximum length of $L_m=(N_b-1)r_m=1.25$ (comparable to the forcing scale l_f) as well as an equilibrium length proportional to $\sqrt{(N_b-1)}r_0=0.04$. The dynamics of the chain is controlled entirely by its elasticity and inertia, described respectively by the Weissenberg number $\mathrm{Wi}=\tau_{\mathrm{chain}}/\tau_f$, where $\tau_{\mathrm{chain}}=6\tau_E/[N_b(N_b+1)]$ provides an estimate of the effective relaxation time of the entire chain [29], and the Stokes number $\mathrm{St}=\tau_p/\tau_\eta$. The inertial relaxation time $\tau_p=2\rho_p a^2/9\rho_f\nu$, where ρ_p and ρ_f are the particle and the fluid densities, respectively; a is the radius of the spherical particle. We use several values of Wi and St to explore the different regimes in the behavior of our elastoinertial chains. We note that the timescales of the elasticity of the links and the inertia of the beads are independent of each other.

III. RESULTS

We begin our study by asking (1) are elastoinertial chains really different from noninteracting inertial particles and (2) does the use of inertial beads, instead of tracer ones as in Ref. [8], modify the dynamics qualitatively? We answer these questions first in the context of the heavy-headed chains [Eqs. (3)–(5)], where the competing influences of elasticity and inertia are most easily illustrated.

In Figs. 2(a) and 2(b), we show representative snapshots of (a) noninteracting inertial particles and (b) heavy-headed chains (the inertial head bead is shown in red, and the inertia-less tail is in black) in a two-dimensional turbulent flow. The underlying vorticity fields, on which for clarity only a random subset of particles or chains is overlaid, are different realizations of the same statistically steady flow. As expected, the inertial noninteracting particles preferentially concentrate in the straining zones of the flow. The behavior of the heavy-headed chains, though, is in stark contrast to this and also differs from the dynamics of the inertia-less elastic chains studied in Ref. [8]. Indeed, in the absence of inertia, elastic chains coil up into vortices and shrink down to tracer-like objects, which then continue to reside inside vortices, whereas in straining regions they are rapidly stretched out until they depart from the underlying straining flow and encounter a vortex. Thus, inertia-less chains get preferentially trapped inside vortices (see Ref. [30] for a movie depicting this behavior), and snapshots such as those in Fig. 2 would show them to be located well inside the core of vortices [8].

Returning to the snapshot of the heavy-headed chains in Fig. 2(b), we see that a majority of them overlap with vortical regions, while, however, remaining elongated, unlike inertia-less chains. The head beads, which are inertial, live on the periphery of the vortices, while their inertia-less elastic tails are pinned to the vortex cores, tracing out a Ferris-wheel pattern. This is especially clear when we look at the arrangement of the chains in and around the vortex visible in the top left corner of Fig. 2(b) (the inset shows a zoomed-in view of this vortex). The elasticity of the tail, which keeps it pinned to the core of the vortex (through the mechanism identified in Ref. [8]), competes with the centrifugal force that pushes the head inertial bead out of the vortex. It is this competition between the two effects which manifests itself in the head beads encircling the edge of the vortices. We refer the reader to Ref. [30] for a movie showing the motion of these chains in the flow, which illustrates this phenomenon—especially the Ferris-wheel pattern—clearly.

These results show that combining an inertial particle with an elastic tail gives rise to dynamics which are very different from that of either a free inertial particle or a purely elastic chain. Such a competition between inertia and elasticity, which dictates the behavior of a heavy-headed chain, also impacts the dynamics of a uniformly inertial chain [Eqs. (1) and (2)], but in a less obvious manner. In Fig. 2(c) which presents a snapshot of uniformly inertial chains (see Ref. [30] for a movie of the time evolution), the core of the strongest vortices are evacuated because of centrifugal forces, while the weaker vortices are still occupied by partially coiled inertial chains. The stark difference between Figs. 2(b) and 2(c) provides a vivid illustration of the importance of the mass distribution of such long objects. For a better appreciation of these effects, we now turn to a more quantitative measurement of the sampling behavior of elastoinertial chains.

A natural way to quantify the relative sampling of vortical and straining regions is to measure the (Lagrangian) Okubo-Weiss parameter

$$\Lambda_c=\frac{\omega_c^2-\sigma_c^2}{4\langle\omega^2\rangle} \tag{7}$$

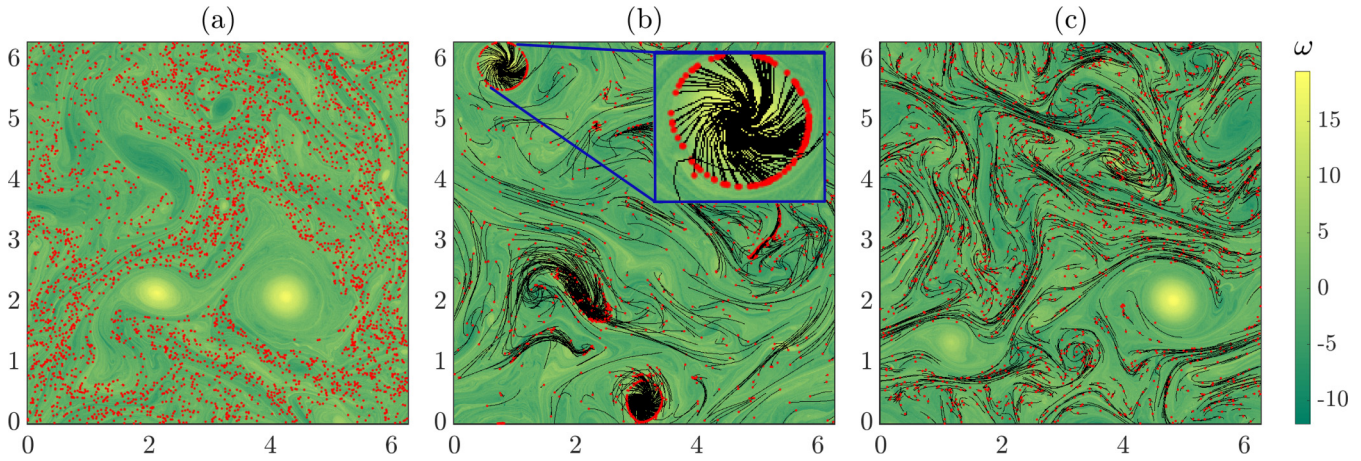

FIG. 2. Representative snapshots of a randomly chosen subset of (a) noninteracting inertial particles, as well as (b) heavy-headed chains and (c) uniformly inertial chains overlaid on the vorticity field. The centers of mass of the chains are shown by red dots [like the free particles in panel (a)] and the chain itself by black lines. The inset in panel (b) shows a zoomed-in view of the vortex located near the top-left corner of this panel. We show results for St = 0.14 and Wi = 1.38 [for panels (b) and (c)].

at the center of mass of the chains along their trajectories. The vorticity ω_c and the strain rate σ_c are measured at the center of mass and normalized by the mean enstrophy $\langle\omega^2\rangle$ of the flow. The sign of this parameter is a signature of the local geometry of the flow: $\Lambda_c > 0$ implies that the center of mass lies in a vortical region, while $\Lambda_c < 0$ is indicative of a straining zone. As is obvious from the definition of Λ_c, extremely small values correspond to regions with comparable amounts of vorticity and straining. As an alternative to Λ_c, one could measure the values of the Okubo-Weiss parameter averaged over all the beads of each chain. We have verified, especially for large Wi, that the two measurements give similar results and lead to the same conclusions.

In Fig. 3 we show the plots of the probability distribution function (PDF) of Λ_c for noninteracting inertial particles and uniformly inertial chains. We consider four values of Wi (0.07, 0.35, 1.38, 6.92) for each of three Stokes numbers: (a) St = 0.14, (b) St = 0.85, and (c) St = 2.84.

For small, but still nonzero Stokes numbers [see Fig. 3(a)], noninteracting inertial particles have a distribution of Λ_c which is negatively skewed, indicating a preferential sampling of straining regions [31]. (Note that uniformly distributed noninteracting *tracers* would show a positively skewed PDF of Λ_c owing to the presence of intense coherent vortices in the flow [27,32].) However, for a chain of inertial beads with the same Stokes number, the effect of the elasticity draws the chain (defined by its center of mass) towards more vortical regions. This is clearly seen in the widening of the right tails of the PDF as Wi increases [Fig. 3(a)].

This effect of elasticity persists, qualitatively, as St is increased to intermediate values, but is considerably weaker [Fig. 3(b)]. On the one hand, the increasing centrifugal forces acting on the chains counteract the tendency of elasticity to entrap them in vortices, causing the large-Wi PDFs to show less positively skewed tails. On the other hand, the noninteracting inertial particles begin to decorrelate from the flow and start to distribute more uniformly, which causes

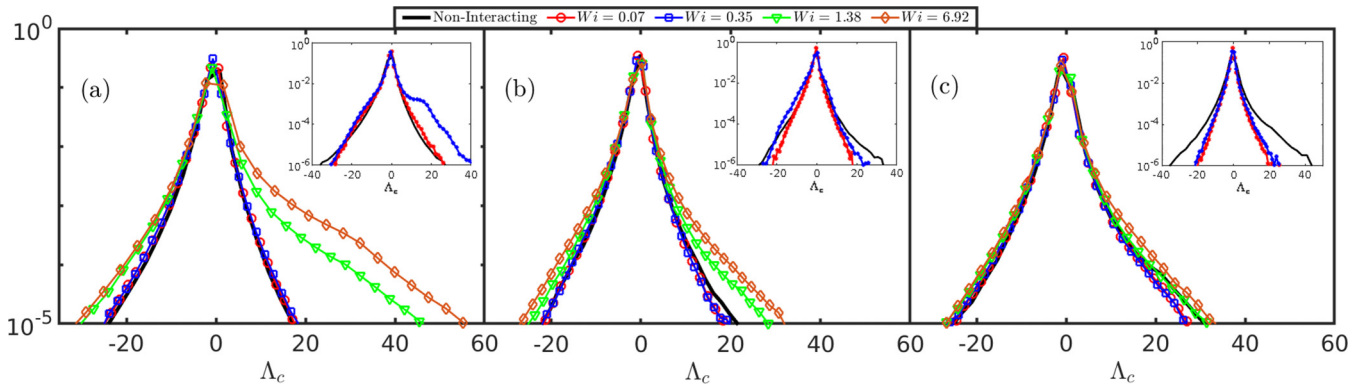

FIG. 3. PDFs of Λ_c measured for uniformly inertial chains with (a) St = 0.14, (b) St = 0.85, and (c) St = 2.84. Curves are plotted for different degrees of elasticity of the chains, as well as for noninteracting inertial particles (see legend). The insets show the same distributions for the heavy-headed chains, but for only two values of Wi.

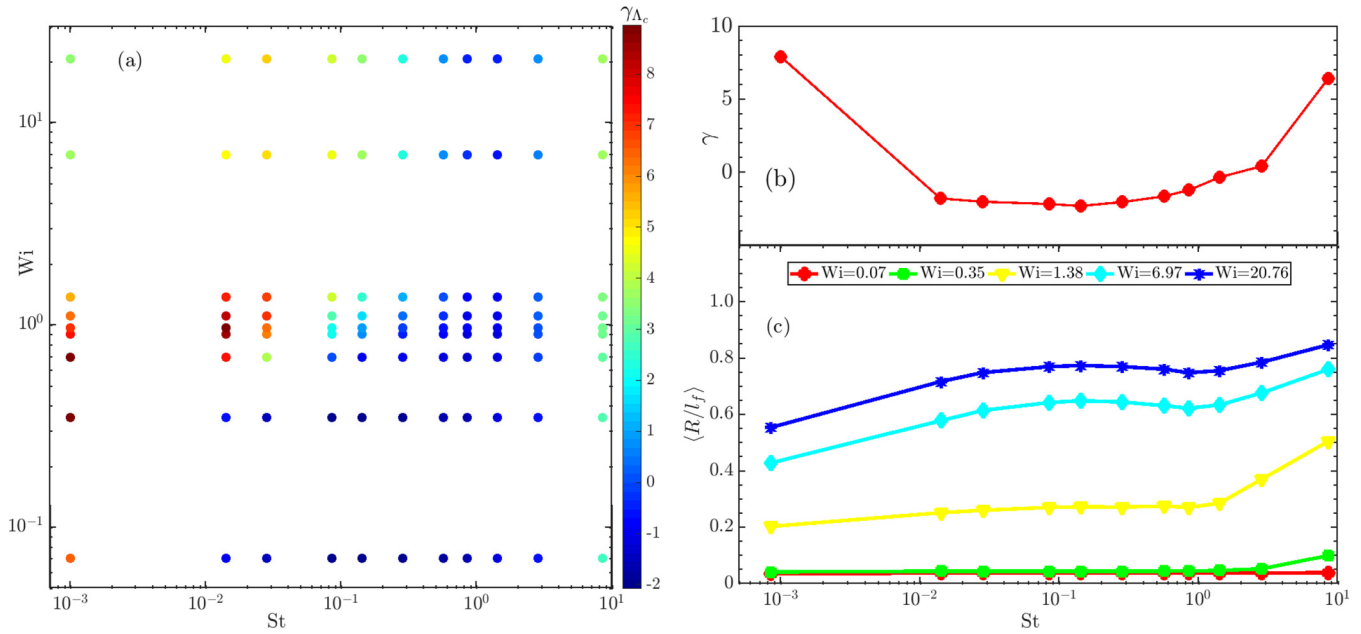

FIG. 4. (a) Pseudocolor plots of the skewness γ of the distribution of Λ_c, in the St-Wi plane, for uniformly inertial chains. For comparison, the same skewness obtained for noninteracting particles is shown in panel (b). We also show in panel (c) the average normalized length of the inertial chains as a function of St for a few representative values of Wi.

the corresponding PDFs of Λ_c to become more positively skewed. The net result is that the effect of Wi weakens, and eventually for large St the PDFs of Λ_c become nearly independent of elasticity [Fig. 3(c)].

Along with the preferential sampling of vortices, increasing Wi also causes a relatively mild oversampling of strong straining regions in comparison with noninteracting particles. This effect is more prominent at small St, as seen in the negative tails of Fig. 3(a). The strong straining regions in two-dimensional turbulence are saddle-like, with a stable direction along which the flow enters and an unstable one along which the flow departs. An inertial point particle in such a saddle region would quickly depart along either branch of the unstable direction. A chain, in contrast, cannot depart as easily: it gets stretched out and oriented along the unstable direction, with the fluid drag at one end of the chain counter-acting that at the other (see the movie in Ref. [30]). The consequence is that an inertial chain spends more time in strong straining zones compared to an inertial point particle. This effect is lost at larger St, as the motion of the chain decorrelates from the instantaneous underlying flow field [Fig. 3(c)].

We now turn to the sampling behavior of a heavy-headed chain. The corresponding PDFs of Λ_c, measured at the head bead, which coincides with the center of mass, are shown in the insets of Fig. 3. For clarity, we present only representative results in each case, for Wi = 0.07 and 0.35. For small St [inset of Fig. 3(a)], the effect of Wi is qualitatively similar to that for a uniformly inertial chain. For larger St, however, the PDFs are quite different. While the elastic tail gets entrapped inside vortices, centrifugal forces push the heavy head bead to their periphery, where the flow is neither intensely vortical nor strongly straining. Consequently, the corresponding PDFs have relatively narrow tails, for both positive and negative values of Λ_c [insets of Figs. 3(b) and 3(c)].

A convenient way of further quantifying the complex dependence of preferential sampling on the inertia and elasticity of a chain is to calculate the skewness of the PDFs of Λ_c,

$$\gamma = \frac{\langle (\Lambda_c - \bar{\Lambda}_c)^3 \rangle}{\langle (\Lambda_c - \bar{\Lambda}_c)^2 \rangle^{3/2}}, \tag{8}$$

where $\bar{\Lambda}_c$ is the average value of Λ_c, as a function of both the Stokes and Weissenberg numbers. For comparison, let us first consider the plot of γ vs St for noninteracting inertial particles shown in Fig. 4(b). Here, γ is negative over intermediate values of St, where there is evidence of preferential concentration (e.g., Ref. [12]), whereas for St $\to 0$ or St $\gg 1$, the homogeneous distribution of these particles ensures that γ is positive (as is the case for tracers).

In Fig. 4(a) we show a pseudocolor plot of the skewness γ in the St-Wi plane for a uniformly inertial chain. We see that when the chain stretches marginally, i.e., for Wi $\ll 1$, γ shows qualitatively the same dependence on St as for noninteracting particles [Fig. 4(b)]. However, when Wi $\gtrsim 1$, the chains are elongated and get trapped by vortices, thereby increasing both the value of γ and the range of St for which $\gamma > 0$.

The difference between a uniformly inertial chain and an inertial-less one [8] can be appreciated by comparing the behavior of γ versus Wi for St around unity with the case of St $\to 0$, in Fig. 4(a). Indeed, for nonzero Stokes numbers, there is a reversal in the sampling behavior, with γ going from negative to positive values with increasing Wi. In contrast, when St $\to 0$, γ remains strictly positive while showing a nonmonotonic dependence on Wi, as has been shown in Ref. [8] and is further discussed below. In the opposite limit of very large St, γ is nearly independent of Wi, in accordance with the PDFs of Λ_c shown in Fig. 3(c).

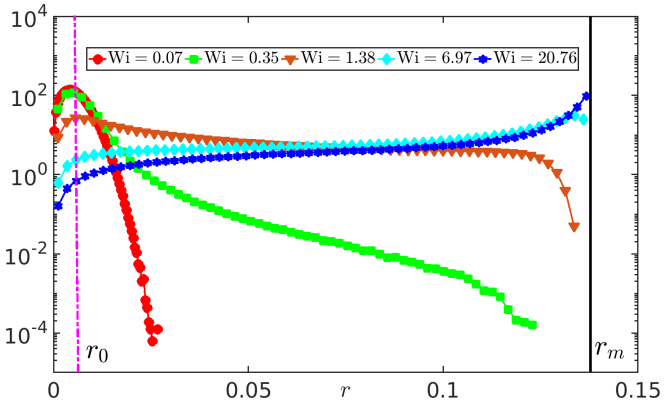

FIG. 5. PDF of the interbead separation r for uniformly inertial (St = 0.14) chains, for different values of Wi (see legend). The solid (black) vertical line corresponds to the maximum link length r_m and the dashed-dot (magenta) line corresponds to r_0 which sets the equilibrium link length. With increasing elasticity, we see the distributions develop broader tails and eventually, at large values of Wi, peak near r_m.

Our arguments, so far, are largely based on the stretching of the chain. It is, therefore, essential to check if stretching indeed happens in the way we suggest. In Fig. 4(c) we show representative plots of the average length of the chain $\langle R \rangle$, normalized by l_f, as a function of St, and for different values of Wi. For a negligible Wi, there is hardly any evidence of stretching. However, as soon as Wi is nonzero, the chain starts stretching much more, in a manner that depends nontrivially on the inertia of the beads.

The variation of the chain length with St occurs in two distinct regimes, which are most clearly visible for the large-Wi case in Fig. 4(c). For St $\lesssim 1$, an inertial chain preferentially samples straining regions of the flow more than an inertial-less one and, therefore, is stretched out more. As St approaches unity, however, the heavy chains begin to decorrelate from the flow, and the degree of sampling of straining regions is reduced [the same is seen for noninteracting particles in Fig. 4(b)]. This is why the chain lengths, especially for large Wi, show a weak local maximum for intermediate values of St ≈ 0.1, where the preferential sampling is strong [see Fig. 4(b)]. In the second regime, of St > 1, the chain lengths again show an increasing trend. This is because, unlike small-St beads, which are well correlated with the flow, the velocity differences between large-St beads do not scale with their separation—even beads that are close to each other can have very different velocities. Therefore, it is more difficult for the elastic links to keep such heavy inertial beads together, and the chain elongates as St increases.

The stretching of the chain is, of course, rooted in the distribution of the lengths of individual links. In Fig. 5 we show a representative plot of this PDF for St = 0.14 and for different values of Wi. When Wi is very small, the PDF is narrow with a peak, as expected, near the equilibrium length scale r_0. With increasing Wi, the PDF initially develops broader tails, but which, for Wi $\lesssim 1$, are still far from the cutoff r_m imposed in our model. As Wi increases beyond unity, however, the distribution starts getting flatter and eventually peaks near to $r = r_m$. For such large-Wi chains, the typical interbead separation is of the order of the vortex size; this limits the ability of the chains to coil into vortices, as successive beads can no longer simultaneously encounter the same vortex (finite N_b acts a restriction on deformability) [8]. This is the reason why γ, for St $\to 0$, shows a peak for Wi ≈ 1 and gradually decreases at large values of Wi [Fig. 4(a)]. For St $\gtrsim 0.1$, however, the centrifugal forces acting on the beads prevent excessive entrapment of chains into vortices, thus eliminating the local maximum in γ and resulting in a more gradual and monotonic increase with Wi.

IV. CONCLUSIONS

Inertia and elasticity are two fundamental properties of extended objects. While the former causes expulsion from vortical regions, as seen for inertial particles, the latter leads to entrapment within vortices, as observed for inertia-less chains. This work has shown, in the context of a model elastoinertial chain, that these competing features interact and result in a nontrivial sampling of a turbulent flow. Moreover, the dynamics of a heavy-headed chain, and its contrast with that of a uniformly inertial one, has shown that a nonhomogeneous mass distribution can lead to a persistent orientation, which keeps the heavier portion of an elastic filament away from vortical regions. Given this, our work, based on model elastic filaments with inertia, serves as a building block for future experimental and numerical studies of the dynamics of extended objects in turbulent flows.

ACKNOWLEDGMENTS

D.V. acknowledges support from the International Centre for Theoretical Sciences (ICTS-TIFR), Bangalore, India. R.S. and S.S.R. acknowledge support of the DAE, Govt. of India, under Project No. 12-R&D-TFR-5.10-1100. S.S.R. acknowledges DST (India) Project No. ECR/2015/000361 for financial support. J.R.P. is grateful for funding from the IITB-IRCC seed grant. J.R.P., S.S.R., and D.V. acknowledge the support of the Indo-French Centre for Applied Mathematics. The simulations were performed on the ICTS clusters Mowgli, Tetris, and Mario as well as the work stations from the project ECR/2015/000361, Goopy and Bagha.

[1] C. Brouzet, G. Verhille, and P. Le Gal, Flexible Fiber in a Turbulent Flow: A Macroscopic Polymer, Phys. Rev. Lett. **112**, 074501 (2014).

[2] G. Verhille and A. Bartoli, 3D conformation of a flexible fiber in a turbulent flow, Exp. Fluids **57**, 117 (2016).

[3] A. Gay, B. Favier, and G. Verhille, Characterisation of flexible fibre deformations in turbulence, Europhys. Lett. **123**, 24001 (2018).

[4] D. Dotto and C. Marchioli, Orientation, distribution, and deformation of inertial flexible fibers in turbulent channel flow, Acta Mech. **230**, 597 (2019).

[5] S. Allende, C. Henry, and J. Bec, Stretching and Buckling of Small Elastic Fibers in Turbulence, Phys. Rev. Lett. **121**, 154501 (2018).

[6] M. E. Rosti, A. A. Banaei, L. Brandt, and A. Mazzino, Flexible Fiber Reveals the Two-Point Statistical Properties of Turbulence, Phys. Rev. Lett. **121**, 044501 (2018).

[7] M. E. Rosti, S. Olivieri, A. A. Banaei, L. Brandt, and A. Mazzino, Flowing fibers as a proxy of turbulence statistics, Meccanica **55**, 357 (2020).

[8] J. R. Picardo, D. Vincenzi, N. Pal, and S. S. Ray, Preferential Sampling of Elastic Chains in Turbulent Flows, Phys. Rev. Lett. **121**, 244501 (2018).

[9] J. Bec, Fractal clustering of inertial particles in random flows, Phys. Fluids **15**, L81 (2003).

[10] J. Bec, A. Celani, M. Cencini, and S. Musacchio, Clustering and collisions of heavy particles in random smooth flows, Phys. Fluids **17**, 073301 (2005).

[11] J. Chun, D. L. Koch, S. L. Rani, A. Ahluwalia, and L. R. Collins, Clustering of aerosol particles in isotropic turbulence, J. Fluid Mech. **536**, 219 (2005).

[12] J. Bec, L. Biferale, M. Cencini, A. Lanotte, S. Musacchio, and F. Toschi, Heavy Particle Concentration in Turbulence at Dissipative and Inertial Scales, Phys. Rev. Lett. **98**, 084502 (2007).

[13] R. Monchaux, M. Bourgoin, and A. Cartellier, Analyzing preferential concentration and clustering of inertial particles in turbulence, Int. J. Multiphase Flow **40**, 1 (2012).

[14] K. Gustavsson and B. Mehlig, Statistical models for spatial patterns of heavy particles in turbulence, Adv. Phys. **65**, 1 (2016).

[15] J. Bec, H. Homann, and S. S. Ray, Gravity-Driven Enhancement of Heavy Particle Clustering in Turbulent Flow, Phys. Rev. Lett. **112**, 184501 (2014).

[16] G. H. Good, P. J. Ireland, G. P. Bewley, E. Bodenschatz, L. R. Collins, and Z. Warhaft, Settling regimes of inertial particles in isotropic turbulence, J. Fluid Mech. **759**, R3 (2014).

[17] S. Sahu, Y. Hardalupas, and A. M. K. P. Taylor, Droplet-turbulence interaction in a confined polydispersed spray: Effect of turbulence on droplet dispersion, J. Fluid Mech. **794**, 267 (2016).

[18] W. W. Grabowski and L.-P. Wang, Growth of cloud droplets in a turbulent environment, Annu. Rev. Fluid Mech. **45**, 293 (2013).

[19] J. Bec, S. S. Ray, E. W. Saw, and H. Homann, Abrupt growth of large aggregates by correlated coalescences in turbulent flow, Phys. Rev. E **93**, 031102(R) (2016).

[20] R. E. Goldstein, Green algae as model organisms for biological fluid dynamics, Annu. Rev. Fluid Mech. **47**, 343 (2015).

[21] F. Gittes, B. Mickey, J. Nettleton, and J. Howard, Flexural rigidity of microtubules and actin filaments measured from thermal fluctuations in shape, J. Cell Biol. **120**, 923 (1993).

[22] A. Choudhary, D. Venkataraman, and S. S. Ray, Effect of inertia on model flocks in a turbulent environment, Europhys. Lett. **112**, 24005 (2015).

[23] A. Gupta, A. Roy, A. Saha, and S. S. Ray, Flocking of active particles in a turbulent flow, arXiv:1812.10288.

[24] R. E. Breier, C. C. Lalescu, D. Waas, M. Wilczek, and M. G. Mazza, Emergence of phytoplankton patchiness at small scales in mild turbulence, Proc. Nat. Acad. Sci. USA **115**, 12112 (2018).

[25] R. B. Bird, C. F. Curtiss, R. C. Armstrong, and O. Hassager, *Dynamics of Polymeric Liquids* (John Wiley and Sons, New York, 1977).

[26] A recent study [33] shows that including bending stiffness in elastic chains with massless (tracer) beads has little effect on the nature of their preferential sampling of a three-dimensional turbulent flow.

[27] P. Perlekar and R. Pandit, Statistically steady turbulence in thin films: Direct numerical simulations with Ekman friction, New J. Phys. **11**, 073003 (2011).

[28] G. Boffetta and R. E. Ecke, Two-dimensional turbulence, Annu. Rev. Fluid Mech. **44**, 427 (2012).

[29] S. Jin and L. R. Collins, Dynamics of dissolved polymer chains in isotropic turbulence, New J. Phys. **9**, 360 (2007).

[30] See Supplemental Material at http://link.aps.org/supplemental/10.1103/PhysRevE.101.053105 for videos showing the evolution of: inertia-less elastic chains, https://www.youtube.com/watch?v=etLuK6ovAqk; heavy-headed chains, https://www.youtube.com/watch?v=zcy1tkB6o9U; and uniformly inertial chains, https://www.youtube.com/watch?v=g0T6JvVVI20.

[31] D. Mitra and P. Perlekar, Topology of two-dimensional turbulent flows of dust and gas, Phys. Rev. Fluids **3**, 044303 (2018).

[32] A. Gupta, P. Perlekar, and R. Pandit, Two-dimensional homogeneous isotropic fluid turbulence with polymer additives, Phys. Rev. E **91**, 033013 (2015).

[33] J. R. Picardo, R. Singh, S. S. Ray, and D. Vincenzi, Dynamics of a long chain in turbulent flows: Impact of vortices, Phil. Trans. R. Soc. A (to be published), arXiv:1912.11431.